

Multi Objective Optimization of Parameters of Torsional Vibration Dampers Considering Damping Effect and Light Weight Design

Can Yang^a, Xiaodong Tan^b, Lin Hua^c, Chihua Lu^d, Yongliang Wang^e and Sheng Wang

Wuhan University of Tech., Wuhan, China

^aCorresponding Author, Email: yangcan@whut.edu.cn

^bEmail: tandengken@163.com

^cEmail: hualin@whut.edu.cn

^dEmail: luchihua@ipowertek.com

^eEmail: wyl8561706@163.com

ABSTRACT:

To reduce the torsional vibration of vehicle power transmission system (VPTS), a torsional vibration model with multiple degrees of freedom (MDOF) of VPTS was established. The scheme of equipping torsional vibration dampers (TVDs) on the driveshaft was employed by the calculation of the forced vibration and the free vibration of the VPTS. The energy method was used to optimize the parameters of single-stage, two-stage parallel, and two-stage series TVDs based on the principle that balances the damping effect and lightweight design. On the basis of this, the parameters of the models incorporating TVD and elastic couplings (ECs) were optimized. Results showed that the proposed method can ensure the damping effects of TVD and realize the lightweight.

KEYWORDS:

Torsional vibration dampers; Two-stage parallel TVD; Two-stage series TVD; Elastic coupling; Lightweight

CITATION:

X. Tan, L. Hua, C. Lu, C. Yang, Y. Wang and S. Wang. 2019. Multi Objective Optimization of Parameters of Torsional Vibration Dampers Considering Damping Effect and Light Weight Design, *Int. J. Vehicle Structures & Systems*, 11(1), 1-6. doi:10.4273/ijvss.11.1.01.

1. Introduction

Research regarding the parameters optimization of the passive torsional vibration dampers (TVD), dynamic vibration absorbers (DVAs), and tuned mass dampers (TMDs) has been well-established. Researches were primarily included the suppression of single degree of freedom (SDOF) system and MDOF system [1-2], nonlinear system [3], continuous system [4], and multiple modes [5]. The mechanical performances of the single-stage and multi-stage TVDs [6-7] and nonlinear DVAs [8], and the continuous parameter DVAs [9], and robust optimization [10], were studied. Most of the investigations conducted to optimize and match the stiffness and damping coefficients of damping devices with a fixed moment of inertia or mass value. There has been little mention of the optimization for inertia or mass values. The TVD inertia values are usually estimated with experience under practical condition. If the inertia values are chosen too small, the damping effects of the TVD may be unsatisfied.

On the other hand, the low power transmission efficiencies will occur with the large inertia values. We wish the larger gyration radius to obtain lightweight TVDs in its structural design with a fixed inertia value. The TVD matched to the vehicle power transmission system (VPTS) generally equipping on the driveshaft which bring a limited outer radius of the TVD, because the installation position is close to the fuel tank. From

this perspective, selecting a smaller inertia value can improve the weight of the TVD. We wish the TVD provides good damping effect but with a smaller inertia value. However, there is no uniform standard for the selection of the inertia values. Fig. 1 shows a two DOF system of a TVD resonating on a main system. J_{eq} and K_{eq} represent the inertia and stiffness of the main system. J_{tvd} , K_{tvd} , and C_{tvd} represent the inertia, stiffness, and damping coefficient of the TVD. M represents the amplitude of the excitation torque. ω represents the excitation frequency and t is time.

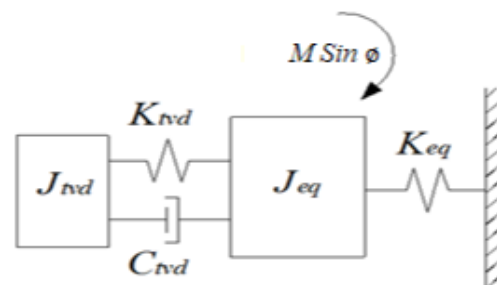


Fig. 1: TVD and a SDOF system

When the TVD parameters are under optimally tuned condition, the maximum value of the ratio of the vibration amplitude of the main system to its static deflection is $\sqrt{1+2/\mu}$ [11], where $\mu = J_{tvd}/J_{eq}$. It can be observed that the maximum vibration amplitude of J_{eq} decreases with the increasing value of μ . As a result, the

weight of TVD runs counter to its good damping effect with a fixed main system, and obtaining the satisfied damping effects and providing acceptable inertia values belong to a multi-objective optimization.

Studies regarding the multi-objective optimization of passive DVAs started relatively late. Marano et al [12] achieved multi-objective optimization by minimizing the maximum standard deviation of the acceleration of a SDOF and the failure probability of TMDs in damped MDOF systems. Seung-Yong et al [13] achieved multi-objective optimization by obtaining the good damping effect and the strong robust performance of the two-stage parallel DVAs, and the robustness of different mass ratio DVAs were compared. Hosseini and Salehipoor [14] achieved multi-objective optimization by minimizing the mass of the DVA and the structure failure probability of the main system through imperialist competitive algorithm. Borges et al [15] achieved multi-objective optimization by minimizing the maximum vibration amplitude of the main system and maximizing the attenuation bandwidth through line-up algorithm.

Regarding the TVDs equipped on the vehicle driveshaft, studies of the multi-objective optimization for damping effect and lightweight are relatively fewer. Our work is based on the severe torsional vibration of a modeled 2nd gear VPTS of a front-engine, rear-drive vehicle. Through the multi-objective optimization model, the parameters of the single-stage, two-stage parallel, two-stage series TVDs, and the models incorporating TVD and ECs are optimized by energy method. The torsional vibration amplitude and maximum torsional elastic potential energy (TEPE) of the VPTS are reduced, and there by the lightweight of the damping devices are realized.

2. MDOF torsional vibration model

Due to complicated structure of a VPTS, the lumped mass method was utilized to simplify the torsional vibration model, which means that a forced vibration model was established by taking the engine output torque as the excitation source. In accordance with the principle of simplification and equivalent calculation method [16], the inertia of each SDOF, the torsional stiffness, and damping coefficient beginning with the intermediate shaft of the gearbox were rendered equal to the engine crankshaft, depending on the transmission ratio of the gear wheels. Accordingly, a 39-DOF torsional vibration model was established, as shown in Fig. 2. The definitions of the inertia terms for the different components of the VPTS represented by each SDOF are listed in Table 1.

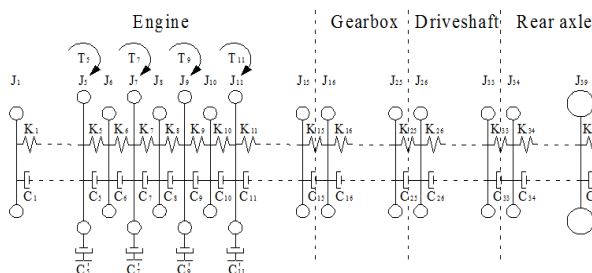


Fig. 2: VPTS torsional vibration model

The torsional vibration equation of the VPTS is,

$$J = T \tag{1}$$

where θ , represent the angular displacement, angular velocity and angular acceleration 39×1 column vectors, respectively. T represents the column vector of the excitation torque. J, C, and K represent the 39×39 inertia matrix, the torsional damping matrix, and the torsional stiffness matrix.

Table 1: Definitions of the different DOF

Symbol	Definition
J_1	Inertia of the torsion damper at the free end of the engine crankshaft
$J_2, J_3, J_{13}, \text{ and } J_{14}$	Inertia values of the stepped shafts
$J_4, J_6, J_8, J_{10}, \text{ and } J_{12}$	Inertia values of the main journal
$J_5, J_7, J_9, \text{ and } J_{11}$	Inertia values of the 4 cylinder crank-connecting rod mechanisms
J_{15}	Inertia values of the flywheel and driving part of the clutch
$J_{16}, J_{17}, J_{18}, \text{ and } J_{19}$	Inertia values of the driven part of the clutch and input shaft of the gearbox
$J_{20} \text{ and } J_{21}$	Inertia values of the intermediate shaft of the gearbox
$J_{22}, J_{23}, J_{24}, \text{ and } J_{25}$	Inertia values of the output shaft of the gearbox
J_{26}	Inertia of the front universal joint and internal spline
J_{27}	Inertia of the front half shaft
J_{28}	Inertia of the intermediate spline
J_{29}	Inertia of the intermediate universal joint
J_{30}, J_{31}, J_{32}	Inertia values of the rear half shaft
J_{33}	Inertia of the rear universal joint
$J_{34} \text{ and } J_{35}$	Inertia values of the main reducer driving and driven bevel gear
J_{36}	Inertia of the differential mechanism
$J_{37} \text{ and } J_{38}$	Inertia values of the two half-axes
J_{39}	Equivalent inertia of wheels and the entire vehicle
$K_i (i = 1, 2, \dots, 38)$	Torsional stiffness between various DOF
K_{39}	Torsional stiffness of tires
$C_i (i = 1, 2, \dots, 38)$	Torsional damping coefficient between various DOF
C_{39}	Torsional damping coefficient of tires
$C'_5, C'_7, C'_9, \text{ and } C'_{11}$	External damping coefficients of the 4 cylinder piston crank-connecting rod mechanisms

3. Forced vibration & free vibration of the MDOF torsional vibration model

The output torque can be presented using Fourier series expansion to determine each harmonic excitation torque. The harmonic superposition method is employed to find the vibration amplitude of each SDOF. As shown in Fig. 3, the vibration amplitudes at the input ends of the gearbox, driveshaft, and rear axle have shown a peak at an engine speed of about 1500 rpm, which represents a resonance phenomenon in the VPTS. This phenomenon can be reduced by a TVD. Prior to optimization, a natural frequency analysis is firstly conducted for the torsional vibration model. Here, an undamped free vibration model is generally utilized to simplify the calculation [17]:

$$J = 0 \tag{2}$$

Their characteristic Eqn. is solved to obtain the third order natural frequency (50.58 Hz) corresponding to the resonance rotation speed at about 1500 rpm.

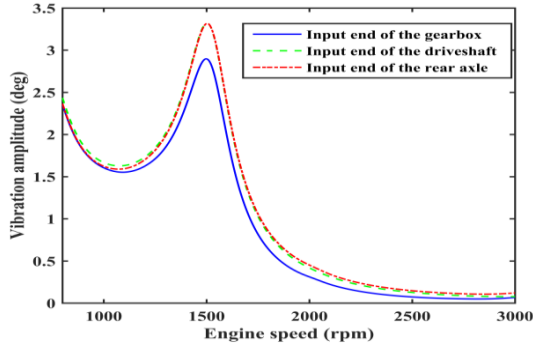


Fig. 3: Amplitudes of different DOF

The corresponding mode shape is shown in Fig. 4, which indicates that the torsional vibration of the complete engine crankshaft (DOF J_1 - J_{15}) is inconspicuous. The clutch (DOF J_{15} and J_{16}) undergoes large deformation due to its low torsional stiffness, which is much less than that of the other shaft segments, the vibration enlarges continuously as the transmission power passes through the input shaft (DOF J_{16} - J_{19}), intermediate shaft (DOF J_{20} and J_{21}), and output shaft (DOF J_{22} - J_{25}) of the gearbox. The complete driveshaft (DOF J_{26} - J_{33}) and main reducer (DOF J_{34} and J_{35}) vibrate increasingly violently. The vibration decreases rapidly as the transmission power passes through the differential mechanism (SDOF J_{36}), half-axes (DOF J_{37} and J_{38}), and reaches the tires (SDOF J_{39}). In a MDOF system, the SDOF having the largest amplitude is equipped with a TVD to absorb the greatest amount of vibration energy.

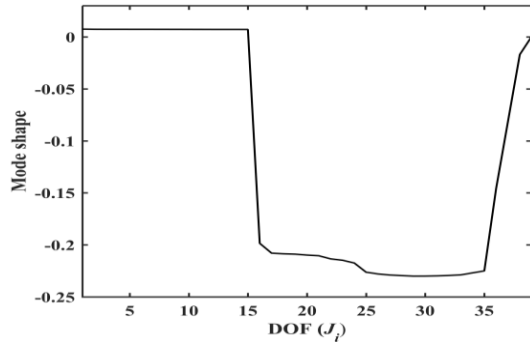


Fig. 4: Third order mode shape of the VPTS

According to the vibration characteristics of the VPTS model and actual situations, a TVD can be optionally equipped at the back end (SDOF J_{32}) of the driveshaft. The mechanical model is shown in Fig. 5, where J'_{tvd} , K'_{tvd} and C'_{tvd} represent the equivalent inertia, torsional stiffness, and torsional damping coefficient of the crankshaft for the TVD, respectively. Then, the torsional vibration equation is established as follows,

$$J_{40 \times 40} \theta_{40 \times 1} = T_{40 \times 1} \quad (3)$$

For enhancing the damping effect, single-stage TVD may be converted into a two-stage parallel or series TVD, the mechanical model of the matched MDOF system is shown in Fig. 6, where J'_{tvd1} , J'_{tvd2} , k'_{tvd2} , C'_{tvd1}

, C'_{tvd2} and C'_{tvd2} represent the equivalent inertias, torsional stiffness, and torsional damping coefficients of the crankshaft for the TVDs, respectively. Then, the torsional vibration equation is established as follows:

$$J_{I,40 \times 40} \theta = T_{41 \times 1} \quad (4a)$$

$$J_{II,41 \times 41} \theta = T_{41 \times 1} \quad (4b)$$

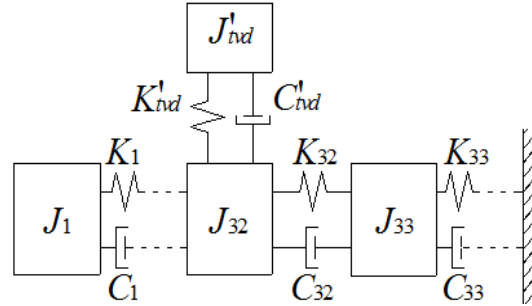


Fig. 5: Mechanical model of the matched MDOF system including single-stage TVD

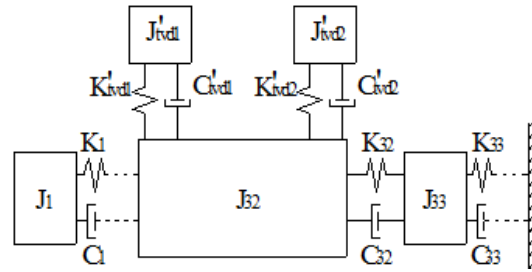


Fig. 6(a): Two-stage parallel TVD

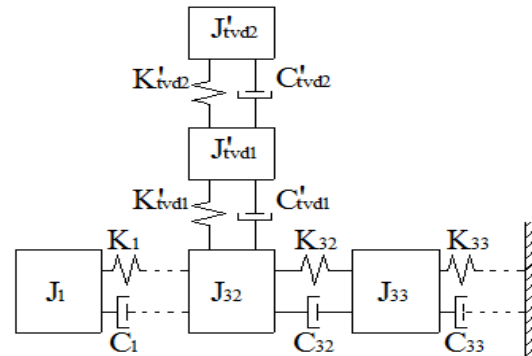


Fig. 6(b): Two-stage series TVD

4. Optimization of TVD parameters

4.1. Optimization model of single-stage TVD

In this model, the inertia, torsional stiffness, and torsional damping coefficient of the TVD are taken as design variables. As the constraint condition, the torsional vibration torque of each shaft section in the torsional vibration system should be less than the corresponding allowable torque and the vibration amplitudes of the DOFs in the rear axle should be less than 0.9 deg. As the boundary condition, the damping co-efficient of rubber is generally in the range 0.05-0.4 N·m·s/rad. Because the torsional vibration of the rear axle dominates the overall NVH performance, the objective function seeks to minimize the maximum TEPE of the rear axle (beginning with component $i = 33$) and the inertia value of equipped TVD. The optimization model is as follows,

$$\begin{aligned}
 & \min E(K_{tvd}, C_{tvd}, J_{tvd}) = \max(F_j), \quad j=1,2 \\
 & \min J_{tvd} \\
 & F_1 = \max_{\substack{\omega=\omega_h \\ 0 \leq t \leq T_1}} \left\{ \sum_{i=33}^{38} \frac{1}{2} K_i * [\theta_i(t) - \theta_{i+1}(t)]^2 + \frac{1}{2} K_{39} * \theta_{39}(t)^2 \right\} \\
 & F_2 = \max_{\substack{\omega=\omega_h \\ 0 \leq t \leq T_2}} \left\{ \sum_{i=33}^{38} \frac{1}{2} K_i * [\theta_i(t) - \theta_{i+1}(t)]^2 + \frac{1}{2} K_{39} * \theta_{39}(t)^2 \right\} \\
 & F_m = \max_{\substack{\omega=\omega_m \\ 0 \leq t \leq T_m}} \left\{ \sum_{i=33}^{38} \frac{1}{2} K_i * [\theta_i(t) - \theta_{i+1}(t)]^2 + \frac{1}{2} K_{39} * \theta_{39}(t)^2 \right\} \\
 & s.t. \quad G(K_{tvd}, C_{tvd}, J_{tvd}) \leq 0
 \end{aligned} \quad (5)$$

Here, F_m is the maximum TEPE of the rear axle when $\omega = \omega_m$, E is the maximum TEPE of the rear axle. We also note that the corresponding frequency ω in the 2nd gear common speed range between 900-2000 rpm was divided into $m - 1$ equal parts, i.e., $\omega_1, \omega_2, \dots, \omega_m$, which represents an even number of points. T_m is the time period of the torsional vibration system when $\omega = \omega_m$. The crankshaft completes two revolutions during single excitation period. The 0.5th order excitation has the largest time period in multiple frequency excitation. Therefore $T_m = 4\pi / (0.5\omega_m)$. $G(K_{tvd}, C_{tvd})$ represents the inequality constraints.

The responses of multiple-order excitation torque are superimposed to obtain the response of each SDOF based on the linear superposition principle using,

$$\theta_{40 \times 1} = \sum_{n=0.5}^{\infty} X_n e^{i(n\omega t + \varphi_n)} \quad (6)$$

where X_n represents the column vector of the vibration amplitudes subjected to the n^{th} order excitation torque of the torsional vibration system. The corresponding steady-state solution of vibration responses is given by the imaginary part of Eqn. (6). The classical optimization method such as linear weighted sum method can be employed to simplify the calculation. The multi-objective optimization may be converted into single-objective optimization using,

$$\min \epsilon_1 \max(F_j) + \epsilon_2 J_{tvd} \quad (7)$$

To realize the lightweight of TVD, ϵ_2 should be greatly larger than ϵ_1 , and the TVD can reach the satisfactory damping effect with a least inertia. For the optimization of parameters for two-stage parallel and series TVDs, the energy function of the rear axle can be obtained based on Eqn. (4), and the objective function is as follows:

$$\begin{aligned}
 & \min E(K_{tvd1}, C_{tvd1}, K_{tvd2}, C_{tvd2}, J_{tvd1}, J_{tvd2}) = \\
 & \max(F_j), j=1,2 \\
 & \min J_{tvd1} + J_{tvd2}
 \end{aligned} \quad (8)$$

where J_{tvd1} and J_{tvd2} , K_{tvd1} and K_{tvd2} , and C_{tvd1} and C_{tvd2} represent the inertias, torsional stiffness, and torsional damping coefficients of the two-stage TVDs, respectively.

4.2. Optimization and analysis of results

It must be noted that, the results of above TVD parameter local optimization are strongly correlated to the initial values selected, and thus a global optimization solver must be employed, and the optimized results are listed in Table 2. As for the single-stage TVD, the rubber cannot provide expected damping, and the dissipated energy is very limited, so that only a very large inertia value TVD can suppress the vibration energy. However,

it is inappropriate to equip the TVD with such large inertia value at the back end of the driveshaft. In contrast, the expected damping coefficients of two-stage parallel and series TVDs are very lesser than the expected damping coefficient of single-stage TVD. The more vibration energy can be dissipated by two-stage TVDs, which need less than half of the inertia value of the single-stage TVD to achieve the same evaluation criterion of damping effect. The parameters in Table 2 were substituted into Eqns. (3) and (4). The calculated vibration amplitudes at the input end of the rear axle are shown in Fig. 7. The amplitude of the VPTS employing single-stage or two-stage TVDs are further reduced between 900-1800 rpm and increases between 800-860 rpm compared with the amplitude with no TVD. Because the 800-900 rpm are generally in first gear, it is reasonable to transfer the vibration energy to uncommonly used speed region. Otherwise, the very large inertia values are needed if 800-2000 rpm is set as the optimization range.

Table 2: Optimized results of the single-stage, two-stage parallel and two-stage series TVDs

Parameter	Single-stage TVD	Two-stage parallel TVD	Two-stage series TVD
K_{tvd1} (Nm/rad)	1642.5031	238.4083	741.4088
C_{tvd1} (Nms/rad)	0.4	0.3456	0.0803
K_{tvd2} (Nm/rad)		502.3032	280.6902
C_{tvd2} (Nms/rad)		0.2552	0.4
J_{tvd1} (Kgm ²)	0.0351	0.0030	0.0107
$J_{tvd1} + J_{tvd2}$ (Kgm ²)		0.0165	0.0151

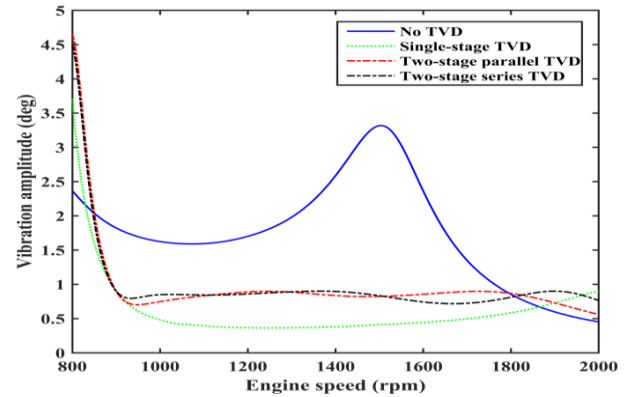


Fig. 7: Vibration amplitudes at the input end of rear axle

5. Optimization of ECs & TVD parameters

5.1. Matching of 1-stage TVD & elastic coupling

To further reduce the weight of the TVD, the TVD and EC can be both considered to equip on the driveshaft. Thus, the parameters of ECs and TVD can be optimized with full play given to the isolation effect of EC and the vibration absorption effect of TVD. We had already investigated the damping effects of different structural schemes combining TVD and ECs on the driveshaft, the optimal installed position of EC should be at the front of the front half shaft. The EC-TVD coupling shock absorber which produces the effects of both EC and TVD should be at back ends of the rear half shaft [18]. The structure of EC-TCD is depicted in Fig. 8, body 1 is inertia ring connected to rubber 4 by vulcanization, body 2 is a lightweight hub connecting rubber 4 and EC 3,

rubber 4 and EC 3 are not connected to each other because of the gap. The mechanical model of the matched VPTS including an EC and an EC-TVD is shown in Fig. 9. K_r and C_r represent the equivalent torsional stiffness and torsional damping coefficients of the crankshaft for the EC. It must be noted that side A should be faced forward and side B should be faced backward.

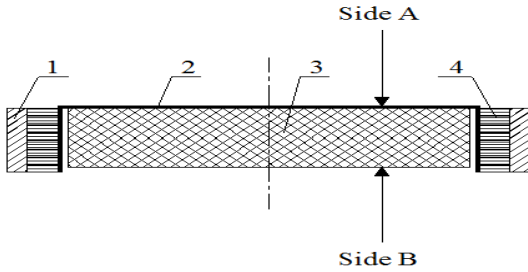


Fig. 8: Schematic diagram of EC-TVD

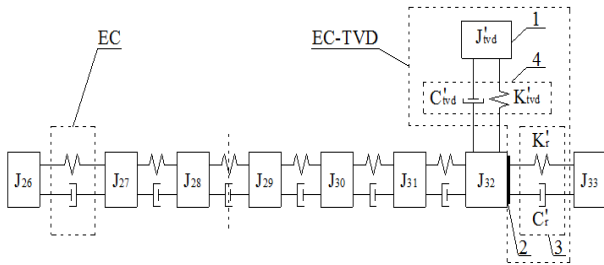


Fig. 9: Schematic diagram of installed position of EC and EC-TVD

5.2. Matching of 2-stage TVDs & elastic coupling

Since single-stage TVD and an EC can be connected together into a coupling shock absorber, an EC-two-stage TVD coupling shock absorber combines an EC and a two-stage parallel or series TVD may be considered to employ. The structures of EC-two-stage TVD are depicted in Fig. 10. This coupling shock absorber requires additional radical space, which introduces installation challenges. The EC-TVD in Fig. 9 can be replaced by EC-two-stage TVD if the condition is satisfied. The mechanical model of the matched VPTS including an EC and an EC-two-stage TVD is shown in Fig. 11.

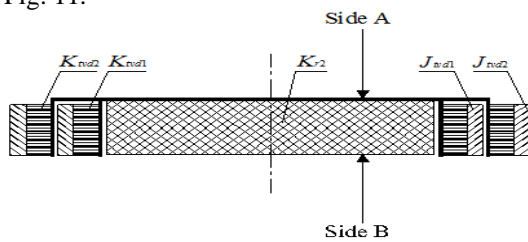


Fig. 10(a): Elastic coupling coupled to two-stage series TVD

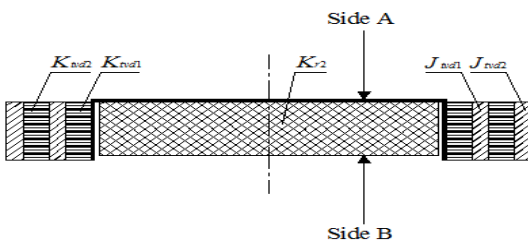


Fig. 10(b): Elastic coupling coupled to two-stage parallel TVD

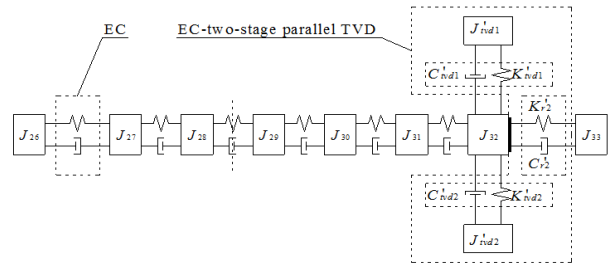


Fig. 11(a): Two-stage parallel TVD and EC

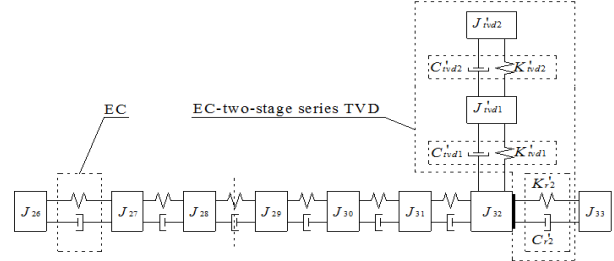


Fig. 11(b): Two-stage series TVD and EC

5.3 Optimization model

For the optimization of parameters for single-stage TVD and ECs shown in Fig. 9, the objective function is as follows:

$$\begin{aligned} \min E(K_{tvd}, C_{tvd}, J_{tvd}, K_{r1}, K_{r2}) &= \max(F_j), j = 1, 2 \\ \min J_{tvd} \end{aligned} \quad (9)$$

Here, K_{r1} is the torsional stiffness of the front EC, K_{r2} is the torsional stiffness of the rear EC. Considering the actual situation, optimization range of EC is set from 1500 N-m/rad to 3000 N-m/rad. The damping of rubber EC is internal damping, which is directly proportional to torsional stiffness of rubber. The value of damping coefficient can be expressed as [19]:

$$C_{r1} = \frac{\psi}{2\pi\omega} 2\pi\omega \quad (10)$$

Here, ψ is the loss coefficient, which is defined as the ratio of dissipated energy to maximum TEPE of the rubber during a period of oscillation (i.e., $T = 2\pi / \omega$). For the optimization of parameters for two-stage TVDs and ECs shown in Fig. 11, the objective function is as follows:

$$\begin{aligned} \min E(K_{tvd1}, C_{tvd1}, K_{tvd2}, C_{tvd2}, J_{tvd1}, J_{tvd2}, K_{r1}, K_{r2}) &= \max(F_j), j = 1, 2 \\ \min J_{tvd1} + J_{tvd2} \end{aligned} \quad (11)$$

5.4. Optimization and analysis of results

Through calculation, the results are shown in Table 3. Compared with Table 2 the optimal stiffness of the TVDs decrease in a certain range. The stiffness of the ECs is at lower boundary values. The inertias of the single-stage TVD the two-stage parallel TVD and the two-stage series TVD decrease 37.08%, 43.68% and 44.84% respectively. The parameters in Table 3 were substituted into Eqns. (3) and (4), and the calculated vibration amplitudes at the input end of the rear axle are shown in Fig. 12. The amplitude of the VPTS employing TVD and EC are reduced considerably between 800-900 rpm, and no obvious changes occur between 900-2000 rpm.

Table 3: Optimized results of the single-stage, two-stage parallel and two-stage series TVDs and ECs

	Single-stage TVD	Two-stage parallel TVD	Two-stage series TVD
K_{tvd1} (Nm/rad)	1198.1151	172.8007	434.0293
C_{tvd1} (Nms/rad)	0.4	0.0851	0.0521
K_{tvd2} (Nm/rad)		292.0315	152.1023
C_{tvd2} (Nms/rad)		0.4	0.2887
K_{r1} (Nm/rad)	1500	1500	1500
K_{r2} (Nm/rad)	1500	1500	1500
J_{tvd1} (Kgm ²)	0.0221	0.0046	0.0056
$J_{tvd1}+J_{tvd2}$ (Kgm ²)		0.0093	0.0083

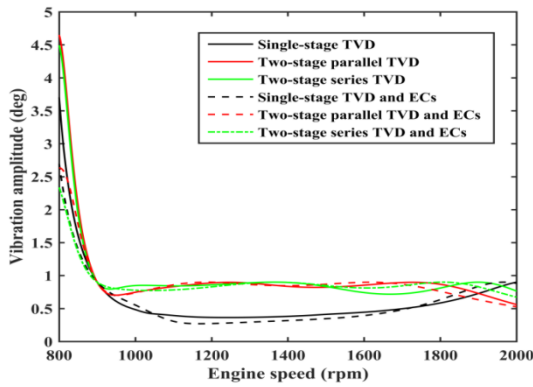


Fig. 12: Vibration amplitudes at the input end of rear axle

6. Conclusions

By considering the damping effects and lightweight of the TVDs, we transferred this problem into the single-objective optimization based on the linear weighted sum method for optimizing the parameters of single-stage, two-stage parallel, two-stage series TVDs, and the models combine ECs and TVD. The two-stage series TVD has the lightweight advantage over the two-stage parallel TVD, and the two-stage parallel TVD has the lightweight advantage over the single-stage TVD. The models combine ECs and TVD have lightweight advantage over the corresponding TVD models, and provided a better damping effect in the 800-900 rpm range.

ACKNOWLEDGMENTS:

The authors would like to thank the Fundamental Research Funds for the Central Universities (WUT: 2016IVA040) for the financial support given to this research.

REFERENCES:

[1] B. Brown and T. Singh. 2011. Minimax design of vibration absorbers for linear damped systems, *J. Sound & Vibration*, 330(11), 2437-2448. <https://doi.org/10.1016/j.jsv.2010.12.002>.

[2] M.B. Ozer and T.J. Royston. 2005. Application of Sherman-Morrison matrix inversion formula to damped vibration absorbers attached to multi-degree of freedom systems, *J. Sound & Vibration*, 283(3), 1235-1249. <https://doi.org/10.1016/j.jsv.2004.07.019>.

[3] R. Viguí and G. Kerschen. 2009. Nonlinear vibration absorber coupled to a nonlinear primary system: A tuning

methodology, *J. Sound & Vibration*, 326(3-5), 780-793. <https://doi.org/10.1016/j.jsv.2009.05.023>.

[4] K. Nagaya and L. Li. 1997. Control of sound noise radiated from a plate using dynamic absorbers under the optimization by neural network, *J. Sound & Vibration*, 208(2), 289-298. <https://doi.org/10.1006/jsvi.1997.1201>.

[5] O. Lavan and Y. Daniel. 2013. Full resources utilization seismic design of irregular structures using multiple tuned mass dampers, *Structural & Multidisciplinary Optimization*, 48(3), 517-532. <https://doi.org/10.1007/s00158-013-0913-x>.

[6] K. Liu and J. Liu. 2005. The damped dynamic vibration absorbers: revisited and new result, *J. Sound & Vibration*, 284(3), 1181-1189. <https://doi.org/10.1016/j.jsv.2004.08.002>.

[7] S. Wenbin and P. Xiaoyong. 2008. Multi-mode and rubber-damped torsional vibration absorbers for engine crankshaft systems, *Int. J. Vehicle Design*, 47(1/2/3/4), 176-188.

[8] S.J. Zhu, Y.F. Zheng and Y.M. Fu. 2004. Analysis of non-linear dynamics of a two-degree-of-freedom vibration system with non-linear damping and non-linear spring, *J. Sound & Vibration*, 271(1-2), 15-24. [https://doi.org/10.1016/S0022-460X\(03\)00249-9](https://doi.org/10.1016/S0022-460X(03)00249-9).

[9] J. Maes and H. Sol. 2003. A double tuned rail damper - Increased damping at the two first pinned-pinned frequencies, *J. Sound & Vibration*, 267(3), 721-737. [https://doi.org/10.1016/S0022-460X\(03\)00736-3](https://doi.org/10.1016/S0022-460X(03)00736-3).

[10] A.D.G. Silva, A.A. Cavalini Jr and V. Steffen Jr. 2016. Fuzzy robust design of dynamic vibration absorbers, *Shock & Vibration*, 2081518, 1-10. <https://doi.org/10.1155/2016/2081518>.

[11] J.P. Den Hartog. 1956. *Mechanical Vibrations*. McGraw-Hill.

[12] G.C. Marano, G. Quaranta and R. Greco. 2008. Multi-objective optimization by genetic algorithm of structural systems subject to random vibrations, *Structural and Multidisciplinary Optimization*, 39(4), 385-399. <https://doi.org/10.1007/s00158-008-0330-8>.

[13] S.Y. Ok, J. Song and K.S. Park. 2009. Development of optimal design formula for bi-tuned mass dampers using multi-objective optimization, *J. Sound & Vibr.*, 322(1-2), 60-77. <https://doi.org/10.1016/j.jsv.2008.11.023>.

[14] R. Hoseini and H. Salehipoor. 2013. Optimum design process of vibration absorber via imperialist competitive algorithm, *Int. J. Structural Stability & Dynamics*, 12(3), 1-15.

[15] R.A. Borges, F.S. Lobato and V. Steffen. 2012. Multi-objective optimization line-up algorithm applied to the design of a nonlinear vibration absorber, *Proc. 10th World Congress on Computational*, 1(1), 1529-1540.

[16] E.J. Nestorides. 2011. *A Handbook on Torsional Vibration*, Cambridge University Press.

[17] S.S. Rao. *Mechanical Vibrations*, 5th Ed., Prentice Hall.

[18] X. Tan, L. Hua and C. Lu. 2017. Study of the optimization of matching between torsional vibration damper and elastic coupling based on energy method, *J. Vibro. Engg.*, 19(2), 769-782. <https://doi.org/10.21595/jve.2016.17135>.

[19] J. Mancuso. 1999. *Coupling and Joints: Design, Selection & Application*, 2nd Ed., Marcell Dekker, New York.